Supported bimetallic Pt-Au nanoparticles: Structural features predicted by molecular dynamics simulations

Brian H. Morrow and Alberto Striolo*
School of Chemical, Biological and Materials Engineering, The University of Oklahoma, Norman, Oklahoma 73019, USA
(Received 8 December 2009; revised manuscript received 9 March 2010; published 19 April 2010)

We have utilized all-atom molecular dynamics simulations to study bimetallic Pt-Au nanoparticles supported by carbonaceous materials at 700 K. Nanoparticles containing 250 atoms with 25%, 50%, and 75% Pt ($Pt_{62}Au_{188}$, $Pt_{125}Au_{125}$, and $Pt_{188}Au_{62}$, respectively) were considered. A single graphite sheet and bundles of seven (10,10), (13,13), and (20,20) single-walled carbon nanotubes were used as supports. It was found that $Pt_{125}Au_{125}$ forms a well-defined Pt core covered by an Au shell, regardless of the support. $Pt_{62}Au_{188}$ exhibits a mixed Pt-Au core with an Au shell. $Pt_{188}Au_{62}$ has a Pt core with a mixed Pt-Au shell. The support affects the atomic distribution. We investigated the percentage of nanoparticle surface atoms that are Pt. Our results show that for $Pt_{62}Au_{188}$ and $Pt_{125}Pt_{125}$, this percentage is lowest when there is no support and highest when carbon nanotubes are supports. We studied the size of clusters of Pt atoms on the nanoparticle surface, finding that the geometry of the support influences the distribution of cluster sizes. Finally, we found that the coordination states of the atoms on the nanoparticle surface are affected by the support structure. These results suggest that it is possible to tailor the distribution of atoms in Pt-Au nanoparticles by controlling the nanoparticle composition and the support geometry. Such level of control is desirable for improving selectivity of catalysts.

DOI: 10.1103/PhysRevB.81.155437 PACS number(s): 61.46.Df

I. INTRODUCTION

Bimetallic catalysts have been the focus of much research because of their chemical versatility and the ability to tune their activity and selectivity by varying their composition and size.[1] For example, bimetallic nanoparticles have been used successfully for methanol oxidation[2,3] and oxygen reduction[4–6] reactions used in fuel cells, for selective hydrogenation,[7–11] and in remediation of groundwater.[12,13] In addition to increasing activity or selectivity, it is possible to use an alloy to replace expensive metals. For example, Fernandez *et al.*[14] found that, when used as catalyst for the oxygen reduction reaction, carbon-supported Pd-Co showed catalytic activity close to that of carbon-supported Pt, the traditionally used, expensive, catalyst. Carbon nanotubes (CNTs), because of their unique properties, are attractive supports for bimetallic catalysts. Pt-Ni nanoparticles on multiwalled carbon nanotubes have been shown to have improved resistance to CO poisoning during methanol oxidation[15] and CNT-supported Pd-Rh has a high activity for the hydrogenation of benzene under mild conditions.[16]

While bimetallic catalysts show great promise, the vast number of potential catalysts poses the problem of identifying the promising candidates while limiting the number of expensive and time-consuming experiments. Computer simulation can aid in the development of new materials. For example, Linic *et al.*[17] used *ab initio* density functional theory (DFT) calculations to formulate a Cu/Ag alloy that has higher selectivity for ethylene epoxidation compared to the traditional Ag catalyst. Studt *et al.*,[18] by performing DFT calculations of hydrocarbon heats of adsorption, identified Ni-Zn alloys as an alternative to the Pd catalysts most commonly used for the selective hydrogenation of acetylene in industry. Both of these predictions were verified experimentally, demonstrating that simulation can be used to develop new catalytic materials. Classical molecular dynamics (MD) simulations can also be used to study catalytic nanoparticles. While classical simulations cannot directly measure catalytic activity, they can examine the structure and dynamics of the nanoparticles at the atomic level. Such data, which cannot always be obtained experimentally, especially under operating conditions, provide insights into the performance of heterogeneous catalysts.

We have previously performed MD simulations of platinum nanoparticles supported by graphite and carbon nanotubes.[19,20] The diffusion of the nanoparticles was found to be 1 order of magnitude slower on carbon nanotubes than on graphite, possibly one reason for the decreased sintering for CNT-supported catalysts found experimentally.[21] We have also found that the geometry of the support affects the morphology of the nanoparticles and the coordination numbers of surface atoms, both of which features play a role in determining catalytic activity. Many other MD studies of supported metal nanoparticles can be found in the literature,[22–38] illustrating the importance of this technique in characterizing heterogeneous catalysts.

Molecular dynamics has also been used to study the properties of bimetallic nanoparticles, including, e.g., the effect of size, structure, and composition on the melting behavior of unsupported Ag-Pd,[39] Au-Pd,[40,41] Cu-Ni,[42] Pd-Pt,[43] and Au-Pt[44,45] nanoparticles. Oviedo *et al.*[46] studied the formation of core-shell nanoparticles composed of combinations of Au, Ag, and Pt atoms. Size and composition effects on the stability of Au-Pt were examined by Xiao *et al.*[47] Mejía-Rosales *et al.*[48] investigated surface sites on Au-Pd nanoparticles. Several other examples exist in the literature of MD simulations of bimetallic nanoparticles.[49–54] Fewer studies have been reported for supported bimetallic nanoparticles. Sankaranarayanan *et al.*[32] studied Pd-Pt, Pd-Rh, and Pd-Cu supported on graphite. Calvo and Balbuena[55] calculated the phonon spectra of graphite-supported Pt-Ag and Pt-Au nanoparticles. Huang *et al.*[22] studied the structure and dynamics

of graphite-supported Cu-Ni and Pt-Au nanoparticles.

In the present paper, we consider supported Pt-Au nanoparticles. In several cases, Pt-Au alloys are more efficient catalysts than monometallic Pt or Au nanoparticles. Dimitratos *et al.*[56] found that carbon-supported Pt-Au had a significantly higher activity for the oxidation of glycerol than carbon-supported Pt. Comotti *et al.*[57] found that, for the oxidation of glucose, pure platinum yields a turnover frequency of 60 h^{-1}, while a Pt-Au alloy with a Au:Pt ratio of 2:1 results in a turnover frequency of 924 h^{-1}. It has also been reported that Pt-Au nanoparticles supported on multiwalled carbon nanotubes show good electrocatalytic activity for methanol oxidation.[58] No molecular dynamics studies of CNT-supported bimetallic nanoparticles exist in the literature. We have performed simulations of Pt-Au nanoparticles containing 25%, 50%, and 75% Pt atoms, supported on graphite and bundles of different-sized CNTs. Our goal is to study the effect of composition and support geometry on the structure of bimetallic Pt-Au nanoparticles, in particular focusing on the atomic-level properties of the nanoparticle surface, which determine the catalytic activity and selectivity.

II. COMPUTATIONAL DETAILS

Nanoparticles were created by carving a 250-atom sphere out of a perfect face-centered cubic lattice. The lattice constant used was that of Pt, 3.92 Å. The lattice constant for Au is slightly larger at 4.08 Å.[59] For each composition considered, the proper numbers of atoms (25%, 50%, or 75%), selected randomly, were designated as Pt atoms, with the remaining atoms designated as Au. Starting from this initial configuration, the nanoparticle was heated from 300 to 1000 K, then cooled to 300 K at a rate of 100 K/ns. The annealed nanoparticle was placed on four supports: a single graphite sheet, a bundle of (10,10) CNTs, a bundle of (13,13) CNTs, or a bundle of (20,20) CNTs. Each of these systems was heated to 1000 K and then cooled to 700 K at a rate of 100 K/ns. All subsequent production runs were performed at 700 K. This temperature is sufficiently high to permit mobility of the metal atoms, but remains below the nanoparticles melting temperature (supported Pt nanoparticles of 250 atoms melt at ~1000 K, Ref. 19). Thus the simulated nanoparticles are at conditions representative of practical catalytic applications (although no reactants or products are considered herein). Further, our results can be considered representative of supported nanoparticles produced at large T (at which condition the atomic distribution is presumably at equilibrium) and then rapidly quenched to room conditions, where the atomic mobility is reduced. Sample snapshots of $Pt_{125}Au_{125}$ nanoparticles supported on the four substrates considered are shown in Fig. 1.

Simulations were performed in the *NVT* ensemble (constant number of particles N, simulation box volume V, and temperature T) at $T=700$ K. All simulations were performed using the large-scale atomic/molecular massively parallel simulator (LAMMPS),[60] implementing the velocity-Verlet algorithm[61] to integrate the equations of motion with a 2 femtosecond time step.

When graphite was used as a support, the carbon atoms were fixed in place. When CNTs were used as support, the carbon atoms were allowed to interact via the Tersoff potential (see below). Periodic boundary conditions were used in all simulations.

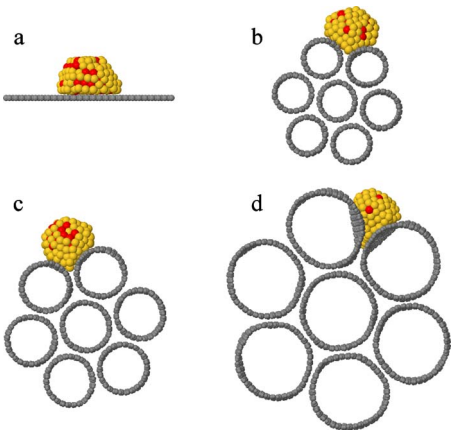

FIG. 1. (Color online) Snapshots of $Pt_{125}Au_{125}$ nanoparticles supported on (a) graphite, (b) (10,10) CNTs, (c) (13,13) CNTs, and (d) (20,20) CNTs. Red (black in print), yellow, and gray spheres represent platinum, gold, and carbon atoms, respectively.

The embedded-atom method (EAM),[62] which has been used to successfully model the properties of both free and supported metal nanoparticles,[63–65] was used to model metal-metal interactions. In the EAM model, the total potential energy is given by

$$U = \sum_i F_i\left(\sum_{j\neq i} \rho_j(r_{ij})\right) + \frac{1}{2}\sum_i \sum_{j\neq i} \phi_{ij}(r_{ij}), \tag{1}$$

where $F_i(\rho)$ is the energy required to embed atom i into the background electron density, ρ_j is the electron density due to atom j, and $\phi_{ij}(r_{ij})$ is the repulsion between the cores of atoms i and j separated by a distance r_{ij}. The force field parameters used to model platinum and gold are those developed by Foiles *et al.*[62] as included in the Pt_u3.eam and Au_u3.eam potential files in the LAMMPS package, respectively.

Carbon-carbon interactions within one CNT are described by the Tersoff potential,[66] which is a three-body potential that has previously been used to model the structural and mechanical properties of carbon nanotubes.[67–71] This force field allows the carbon atoms in CNTs to vibrate and move in response to the presence of the metal nanoparticles.

Carbon-carbon interactions between atoms in different CNTs were modeled using the 12–6 Lennard-Jones potential, using the parameters $\varepsilon_{C\text{-}C}=0.0024$ eV and $\sigma_{C\text{-}C}=3.4$ Å.[72] The Lennard-Jones potential was also used to model metal-carbon interactions. Starting with the metal-metal parameters developed by Agrawal *et al.*,[73] the metal-C parameters were then obtained using the C-C parameters and the Lorentz-Berthelot mixing rules.[61] The metal-C parameters thus obtained are $\varepsilon_{Pt\text{-}C}=0.0408$ eV, $\sigma_{Pt\text{-}C}=2.936$ Å, $\varepsilon_{Au\text{-}C}=0.0332$ eV, and $\sigma_{Au\text{-}C}=2.985$ Å. Recent *ab initio* DFT simulation results suggest that these parameters for metal-carbon interactions (specifically for Pt-C interactions) may be too weak.[74] We previously performed simulations to as-

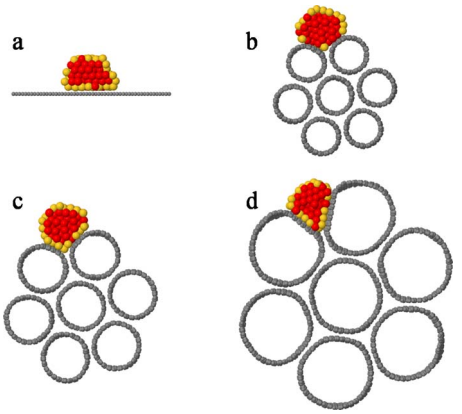

FIG. 2. (Color online) Same as Fig. 1, but with half of the nanoparticles removed to provide a cutaway view of the interior of the nanoparticles.

sess the extent by which uncertainties in metal-carbon interactions affect MD results. We found that, except for small nanoparticles or for Pt nanoparticles supported on carbon nanotubes with large curvature (small radius), the Lennard-Jones epsilon value does not significantly affect the structure of the supported nanoparticle.[75] Because the simulations performed here are conducted for rather large nanoparticles, we expect that the force fields implemented yield semiquantitative results for the nanoparticle morphology.

III. RESULTS AND DISCUSSION

A. Atomic segregation within nanoparticles

Snapshots for $Pt_{125}Au_{125}$ supported nanoparticles, with half of the nanoparticles not shown to provide a view of the interior of the nanoparticles, are shown in Fig. 2. As can be seen from the snapshots, the gold atoms tend to segregate to the nanoparticle surface, leaving a Pt-rich core. The geometry of the support affects to some extent the atomic segregation. For all four supports, there is a core of Pt atoms surrounded by a shell of Au atoms interspersed with a few Pt atoms, but the supports deform the nanoparticles, thus yielding different atomic distributions compared to those observed for unsupported nanoparticles of similar composition. The support curvature in some cases enhances this effect (see, e.g., panel b in Fig. 2 where it appears that Pt atoms, and not Au ones, are in contact with the CNTs). To quantify the distribution of the atoms within the metal nanoparticles, we calculated the average number of atoms of each type as a

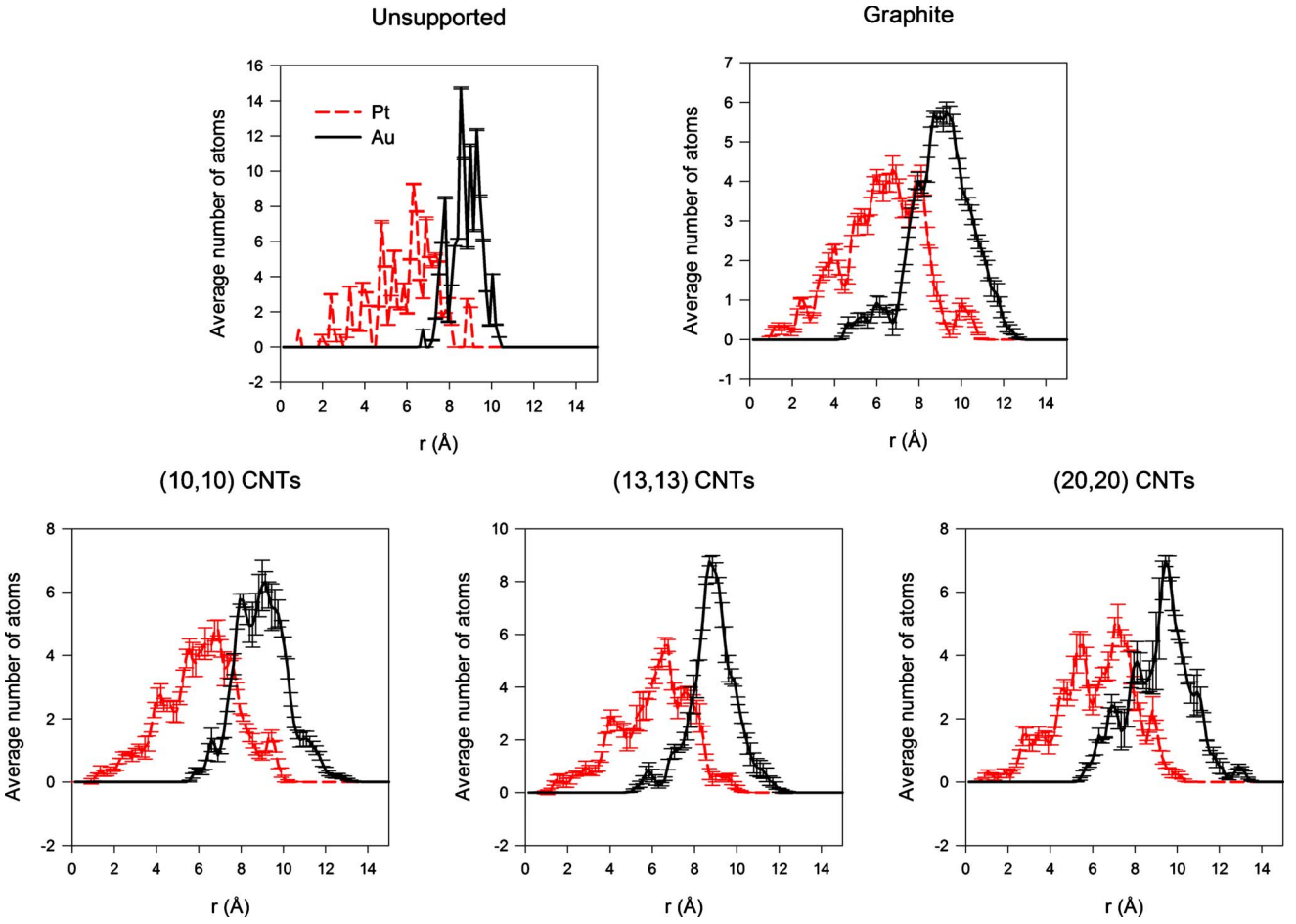

FIG. 3. (Color online) Number of Pt (red) and Au (black) atoms as a function of distance from the nanoparticle center of mass for $Pt_{125}Au_{125}$ in vacuum (unsupported) and on the four carbonaceous supports considered. The statistical uncertainty is estimated as one standard deviation.

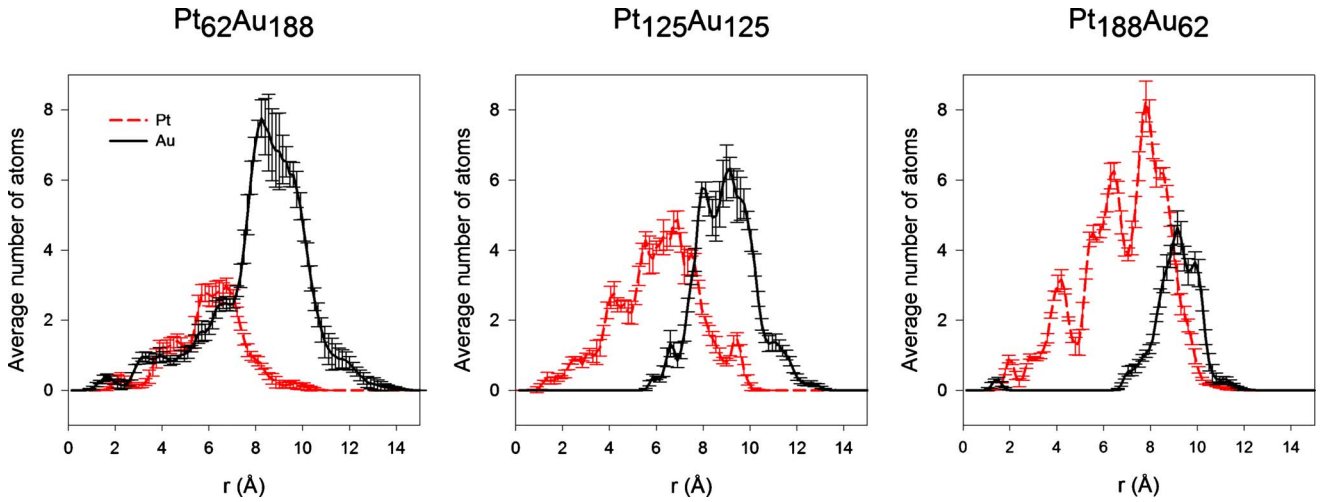

FIG. 4. (Color online) Number of Pt (red) and Au (black) atoms as a function of distance from the nanoparticle center of mass for $Pt_{62}Au_{188}$, $Pt_{125}Au_{125}$, and $Pt_{188}Au_{62}$ nanoparticles supported by bundles of (10,10) CNTs. The statistical uncertainty is estimated as one standard deviation.

function of the distance from the nanoparticle center of mass. These results for $Pt_{125}Au_{125}$ are reported in Fig. 3.

Although the results are qualitatively similar for the nanoparticle in vacuum (unsupported) or supported on each carbonaceous material studied here [graphite, (10,10), (13,13), and (20,20) CNTs], some quantifiable differences can be observed as a function of the support. Closer to the center of mass of the nanoparticle, only Pt atoms are present. Au atoms can be found starting at ~4 Å when the nanoparticle is supported by graphite and at around 5–6 Å on CNTs and in vacuum. The Au atoms are concentrated farther from the nanoparticle center of mass, with the peak in their distribution occurring at around 9 Å. When the nanoparticle is unsupported, the atomic distributions show sharp peaks, reflecting the symmetric lattice structure of the metal atoms. When supports are present, the symmetry is broken and radially averaging the distribution of the atoms results in fewer, smoother peaks. All five systems clearly indicate a well-defined Pt-Au core-shell structure, with the support affecting, albeit slightly, the radial distribution of the metal atoms. Despite the statistical uncertainty intrinsic in our calculations (the error in Fig. 3 is estimated as one standard deviation from the five independent simulations conducted for each system), some of the differences observed for the atomic distribution within the nanoparticles are relevant. For example, at ~6 Å, the number of Pt atoms is lowest on (20,20) CNTs and the number of Au atoms at ~8.5 Å is almost two atoms higher on (13,13) CNTs than on any other support. We do not examine these differences in any more detail as small changes of the arrangement of the interior atoms are not expected to have a significant effect on the catalytic activity of the nanoparticle. The segregation of the Au atoms to the nanoparticle surface is driven both by the fact that Au atoms have larger diameters than Pt atoms and because Au has a lower surface energy than Pt. Thermodynamic models[47] and MD simulations[44,47,76] have predicted the formation of Pt-Au core-shell nanoparticles. Reyes-Nava *et al.*[77] used atomic properties of constituent elements to predict trends for surface segregation in bimetallic nanoparticles and supported their predictions with MD and DFT calculations. Their results indicate an Au-rich shell in Pt-Au nanoparticles, in agreement with our results. Pt-Au core-shell nanoparticles have been observed experimentally,[78–81] although Au-Pt core-shell nanoparticles can also be prepared.[82,83]

As detailed below, and not surprisingly, our simulations show that the atomic distribution within the nanoparticles

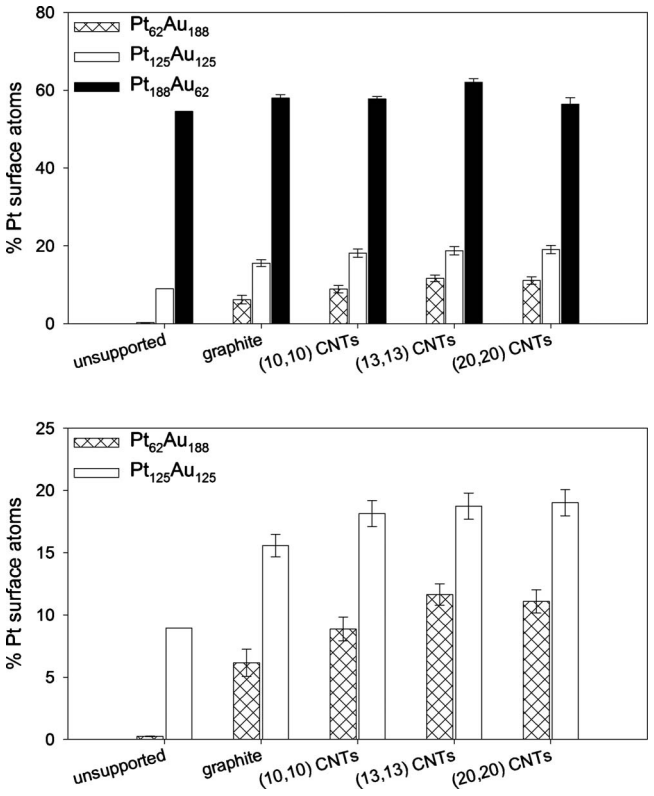

FIG. 5. Average nanoparticle surface composition as a function of support. Three nanoparticle compositions are considered: $Pt_{62}Au_{188}$, $Pt_{125}Au_{125}$, and $Pt_{188}Au_{62}$. The bottom panel provides an expansion of the results shown in the top panel for $Pt_{62}Au_{188}$ and $Pt_{125}Au_{125}$ nanoparticles.

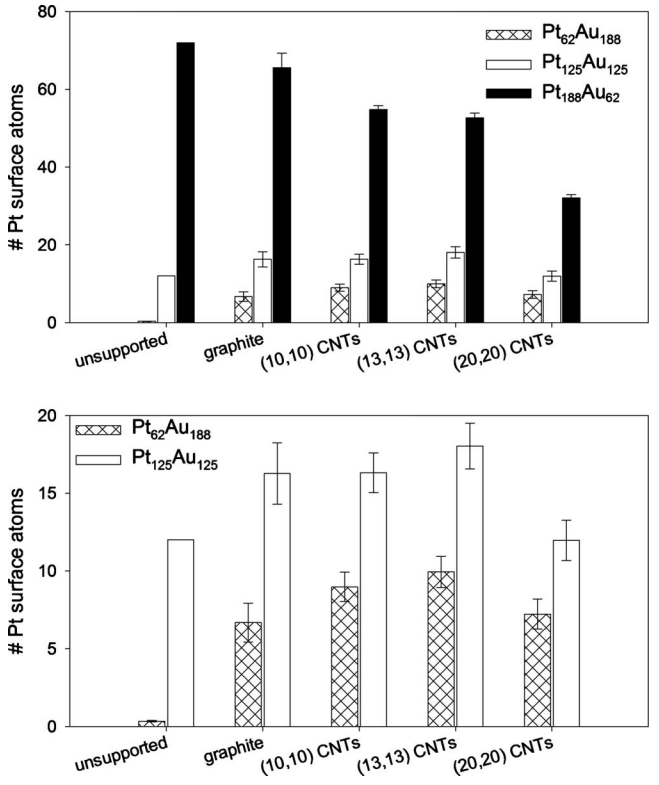

FIG. 6. Average number of Pt atoms on the nanoparticle surface. Three nanoparticle compositions are considered: $Pt_{62}Au_{188}$, $Pt_{125}Au_{125}$, and $Pt_{188}Au_{62}$. The bottom panel provides an expansion of the results shown in the top panel for $Pt_{62}Au_{188}$ and $Pt_{125}Au_{125}$ nanoparticles.

changes more significantly when the nanoparticle composition varies. In Fig. 4, we report the atomic distribution as a function of distance from the center of mass for $Pt_{62}Au_{188}$, $Pt_{125}Au_{125}$, and $Pt_{188}Au_{62}$ nanoparticles, all supported by (10,10) CNTs. Results for $Pt_{62}Au_{188}$ and $Pt_{188}Au_{62}$ on all the supports are not shown for brevity because the atomic distributions are qualitatively similar for all cases studied. Specifically, in the case of $Pt_{62}Au_{188}$, there are not enough Pt atoms within the nanoparticle to form a well-defined core-shell structure. There are Au atoms found at less than 2 Å from the center of mass, compared to $Pt_{125}Au_{125}$ where Au atoms are at least 5 Å away from the center of mass. The distributions of Pt and Au atoms are nearly equal within ~7 Å of the center of mass, indicating that they are evenly mixed near the center of the nanoparticle. More than 7 Å away from the center of mass, the nanoparticle is almost exclusively composed of Au atoms. As discussed above, $Pt_{125}Au_{125}$ nanoparticles display a Pt-Au core-shell structure. In the case of $Pt_{188}Au_{62}$ nanoparticles, aside from a small peak near 2 Å, there are no Au atoms present within 7 Å of the nanoparticle center of mass. At ~9 Å from the center of mass, Pt and Au are mixed, with slightly more Au atoms present at any given distance. Summarizing, our results show that $Pt_{125}Au_{125}$ nanoparticles consist of a core almost entirely composed of Pt and a shell consisting almost entirely of Au. When fewer Pt atoms are present, as in $Pt_{62}Au_{188}$, a mixed Pt-Au core covered by a nearly pure Au shell is formed. When the nanoparticle is predominantly Pt, as in $Pt_{188}Au_{62}$, the structure

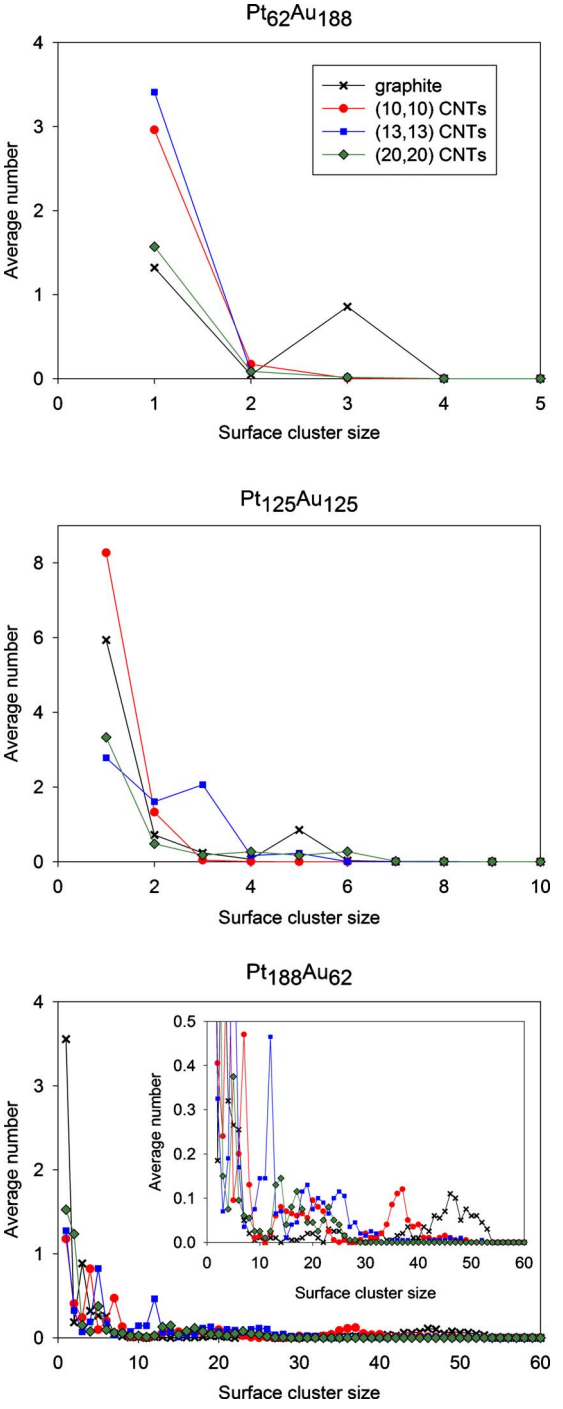

FIG. 7. (Color online) Average number of surface Pt clusters of given size, for $Pt_{62}Au_{188}$ (top), $Pt_{125}Au_{125}$ (middle), and $Pt_{188}Au_{62}$ (bottom). Error bars are not shown for clarity, but are ± ~0.2–0.3 for surface-cluster sizes less than ~4 and ± ~0.01–0.02 for the larger cluster sizes found on $Pt_{188}Au_{62}$

consists of a pure Pt core covered by a mixed Pt-Au shell.

B. Nanoparticle surface characterization

The different distributions of Pt and Au atoms in the nanoparticles' shells suggest that the atomic distribution on the nanoparticle surface may depend on the nanoparticle

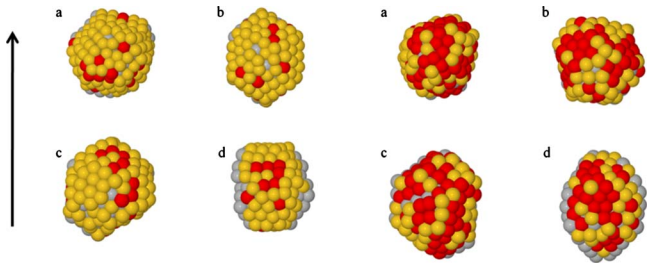

FIG. 8. (Color online) Snapshots of $Pt_{125}Au_{125}$ (left panel) and $Pt_{188}Au_{62}$ (right panel) on (a) a single graphite sheet, (b) (10,10) CNTs, (c) (13,13) CNTs, and (d) (20,20) CNTs. Pt and Au surface atoms are represented by red and yellow spheres, respectively. Metal atoms that are not on the nanoparticle surface are colored gray. Carbon atoms are not shown for clarity. Arrow indicates the direction of the CNT axes.

composition and to some extent also on the support. Because of the importance of such results in catalysis, we quantify herein the distribution of atoms on the nanoparticle surface. In Fig. 5, we report the percent of surface atoms that are platinum for each of the three compositions considered, as a function of the support. The values reported are the averages of five simulations and the error bars represent one standard deviation in each direction. In the case of $Pt_{188}Au_{62}$, our calculations show the percentage of surface atoms that are platinum ranges from 55% for unsupported nanoparticles to 62% for nanoparticles supported by (13,13) CNTs, without a clear trend as a function of support. For both $Pt_{62}Au_{188}$ and $Pt_{125}Pt_{125}$ nanoparticles, the percentage of surface atoms that are platinum is lowest when there is no support, increases on graphite, and is highest when CNTs are used as supports, increasing slightly as the CNT radius increases, except for $Pt_{62}Au_{188}$, where the percentage decreases slightly on (20,20) CNTs. As can be seen in detail in the bottom panel of Fig. 5, for the $Pt_{62}Au_{188}$ nanoparticle, the percentage ranges from 8.9% on (10,10) CNTs to 11.6% on (13,13) CNTs. For the $Pt_{125}Au_{125}$ nanoparticle, the percentages range from 18.1% on (10,10) CNTs to 19.0% on (20,20) CNTs.

To explicitly quantify the results for the surface composition, in Fig. 6, we report the number of Pt atoms on the surface of the three nanoparticles as a function of the support. The results in Fig. 6 are quite important. For example, in the $Pt_{62}Au_{188}$ nanoparticle in vacuum <1–2 of the Pt atoms are on the surface, while when the same nanoparticle is supported by (13,13) CNTs, $\sim$10 of the 62 Pt atoms ($\sim$16% of the Pt atoms) are located on the nanoparticle surface. As another example, in the $Pt_{188}Au_{64}$ nanoparticle on graphite, $\sim$35% of the Pt atoms are on the nanoparticles surface, but when the same nanoparticle is supported on bundles of (20,20) CNTs, only $\sim$17% of the Pt atoms are available for catalytic applications. Note that the total number of Pt atoms on the nanoparticles surface can change even though the percentage of Pt atoms on the surface does not vary because when the support changes, due to the effective surface roughness, the nanoparticles rest between contiguous nanotubes and the total number of surface atoms changes compared to when the nanoparticles rest on flat graphite. We do not count as "surface atoms" those metal atoms that are in contact with the carbon supports. As the number of Pt atoms on the surface varies, their coordination state (as discussed below) also varies. This effect, when considered combined for the large number of nanoparticles typically used for practical catalytic applications, will yield macroscopic effects on both catalytic activity and selectivity. Overall, the results in Figs. 5 and 6 suggest that for Pt-Au bimetallic nanoparticles, it is possible to control the nanoparticle surface features by choosing the appropriate support.

Even more important for catalytic applications is the coordination state of the Pt atoms on the nanoparticle surface. In Fig. 7, we report the average number of Pt atom clusters found on the nanoparticle surface as a function of the number of Pt atoms in the cluster. Error bars are not shown for clarity, but are $\pm\sim 0.2$–0.3 for surface-cluster sizes less than $\sim$4 and are much smaller ($\pm\sim 0.01$–0.02) for the larger cluster sizes found on $Pt_{188}Au_{62}$. A "surface cluster" is defined as a group of surface Pt atoms that are neighbors with each other. For example, if atoms 1 and 2 are neighbors, atoms 2 and 3 are neighbors and atoms 2 and 4 are neighbors, then atoms 1–4 are part of one surface cluster of size 4. On $Pt_{62}Au_{188}$ nanoparticles, we predominantly see single-atom clusters when CNTs are supports. When graphite is the support, clusters of three atoms are present. On $Pt_{125}Au_{125}$ nanoparticles, there are no clusters larger than six Pt atoms and the support influences the distribution of cluster sizes. For example, there are $\sim$3 times as many clusters of five atoms when the support is graphite compared to when the support is CNTs. The most pronounced differences are found for $Pt_{188}Au_{62}$ nanoparticles, in which case the support geom-

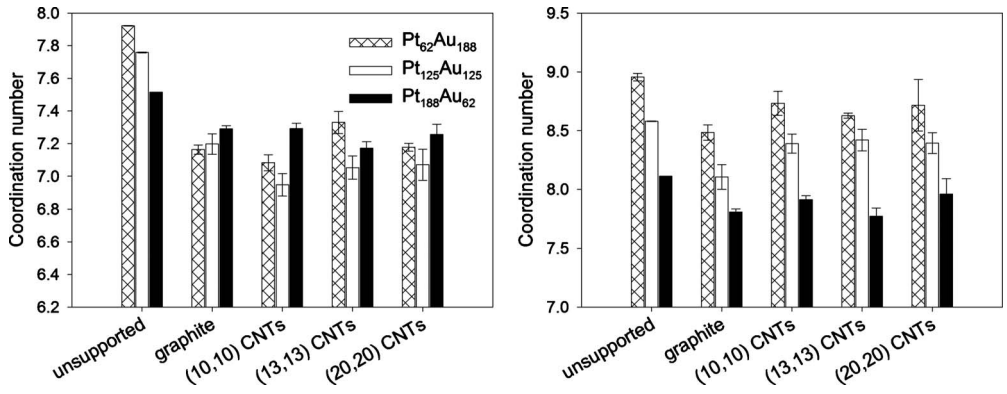

FIG. 9. Average coordination number of all surface atoms (left) and Pt surface atoms (right) with any other atom.

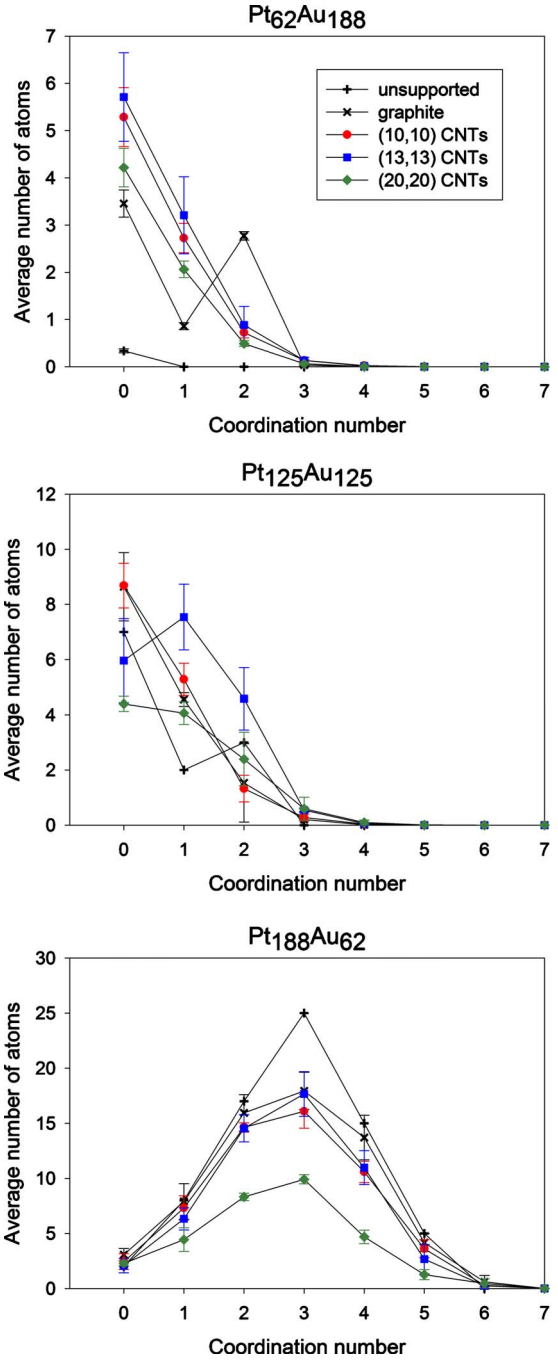

FIG. 10. (Color online) Average number of surface Pt atoms of a given coordination number with other Pt surface atoms. Results are shown for $Pt_{62}Au_{188}$ (top), $Pt_{125}Au_{125}$ (middle), and $Pt_{188}Au_{62}$ nanoparticles (bottom).

etry appears to play a large role in the distribution of atoms on the nanoparticles' surface. When the support is graphite, there is a peak around cluster size 45–50, when the support is (10,10) CNTs, the peak shifts to around 35–40 Pt atoms, and when the support is (13,13) CNTs, there is a high concentration of surface clusters of 12 Pt atoms.

Snapshots of $Pt_{125}Au_{125}$ and $Pt_{188}Au_{62}$ nanoparticles, with the supporting carbon atoms not shown for clarity, are shown in Fig. 8. These snapshots qualitatively confirm the results discussed above and additionally indicate that the coordination state of the surface Pt atoms is affected by the support and by the nanoparticle composition. Specifically, $Pt_{125}Au_{125}$ shows chains of Pt and isolated Pt atoms on the surface, while the surfaces of the $Pt_{188}Au_{62}$ nanoparticles have larger clusters of Pt atoms and fewer isolated Pt atoms.

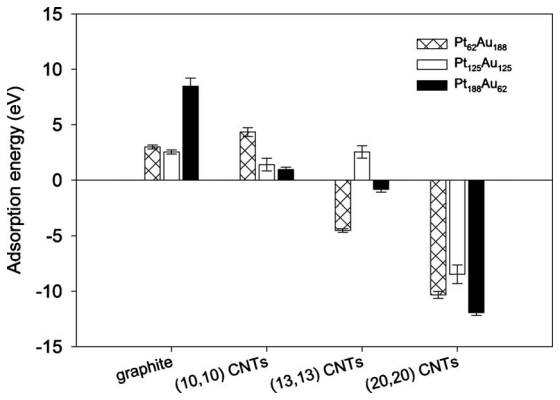

FIG. 11. Nanoparticle adsorption energy on the four supports.

To further examine the nanoparticles' surfaces, we calculated the coordination numbers of the surface atoms. In Fig. 9, we report the average coordination numbers of all surface atoms (left panel) and of the Pt surface atoms (right panel). We point out that the data in Fig. 9 correspond to the coordination with any other metal, either Au or Pt. The values reported are the averages of five simulations and the error bars represent one standard deviation in each direction. For unsupported nanoparticles, the average coordination number decreases as the Pt content of the nanoparticle increases, both when all surface atoms and only Pt surface atoms are considered (left and right panels, respectively). When all surface atoms are considered, the average coordination number is lower when the nanoparticle is supported than when it is not, but there is no clear trend in the variations of the average coordination number as the support changes. When the average coordination number of the Pt surface atoms is calculated for a given composition, the unsupported nanoparticles have the highest average coordination number and nanoparticles on CNTs have higher average coordination number than those on graphite.

We have also calculated the Pt-Pt coordination number of Pt atoms on the surface; that is, for every Pt surface atom, we count the number of nearest-neighbor Pt surface atoms. This is important to quantify because different sizes of groups of Pt atoms can catalyze different, sometimes competitive, chemical reactions. The average number of surface Pt atoms having a given Pt-Pt coordination number is reported in Fig. 10. A Pt-Pt coordination number of zero represents a single surface Pt atom surrounded by gold atoms. Surface Pt atoms with coordination number 1 are arranged in pairs surrounded by gold atoms, etc.

For $Pt_{62}Au_{188}$, the distribution of coordination numbers is similar on all three sizes of CNTs studied. For these nanoparticles, most of the surface Pt atoms are surrounded only by Au atoms. On graphite, however, we find a larger number of Pt surface atoms with a Pt-Pt coordination number of 2, meaning that on graphite, there is a larger concentration of

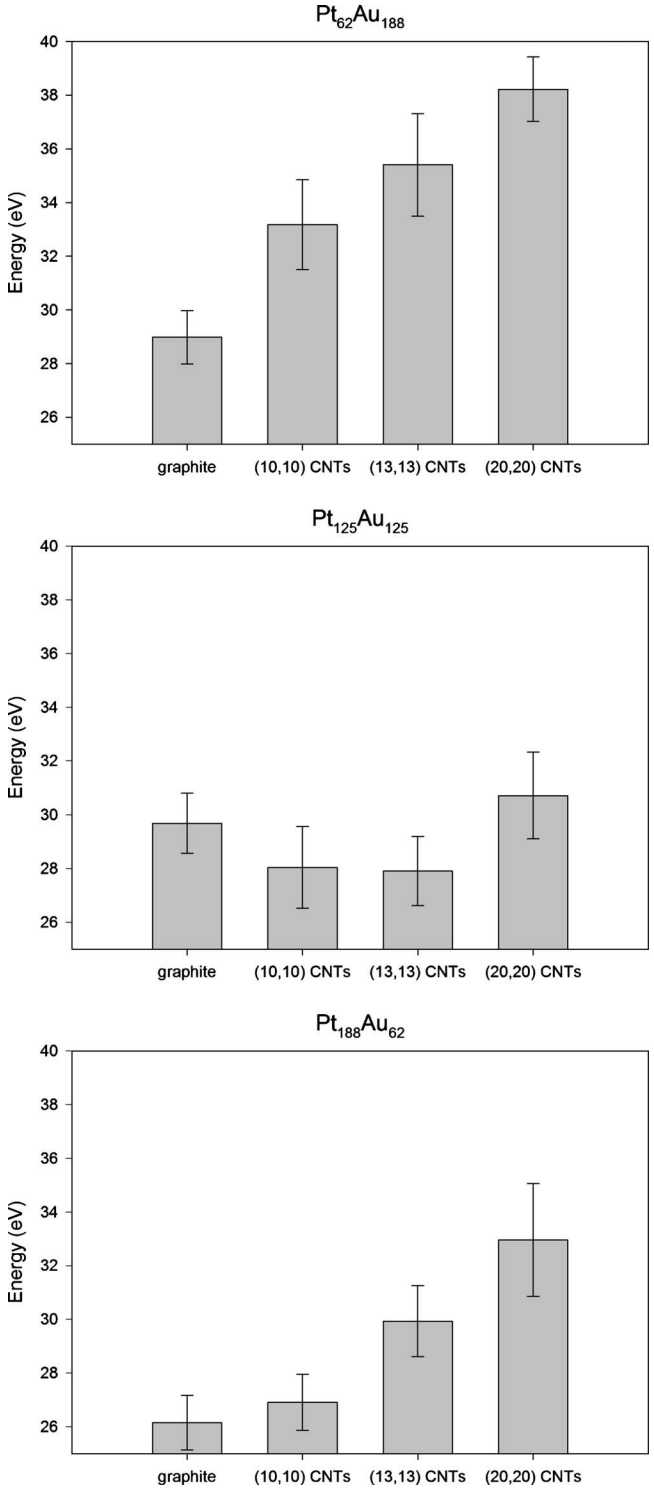

FIG. 12. Nanoparticle deformation energy.

islands of three Pt atoms on the nanoparticle surface. For $Pt_{125}Au_{125}$, the nanoparticle on (13,13) CNTs has the highest concentration of atoms with a coordination number of 1 (pairs of Pt atoms on the nanoparticle surface). For $Pt_{188}Au_{62}$, on all supports as well as for the unsupported nanoparticle, the distribution increases as the coordination number increases from 0 to 3, then decreases as the coordination number increases further. The distribution for coordination numbers 2–4 is similar for nanoparticles on graphite, (10,10) CNTs and (13,13) CNTs, but is ~50% lower for nanoparticles on (20,20) CNTs. At the lower Pt compositions, $Pt_{62}Au_{188}$ and $Pt_{125}Au_{125}$, there are fewer Pt atoms on the surface (see Fig. 6), so many of the Pt atoms are isolated or only have 1 or 2 surface Pt neighbors. As the coordination number increases, the number of Pt atoms having that coordination number decreases. There are many more Pt atoms on the surface of $Pt_{188}Au_{62}$ nanoparticles, so a smaller percentage compared to $Pt_{62}Au_{188}$ and $Pt_{125}Au_{125}$ is isolated or have only 1 or 2 surface Pt neighbors. As the coordination number increases past 3, it is more difficult for an atom to have a large number of neighbors on the surface. This explains the maximum at coordination number 3 in the case of the $Pt_{188}Au_{62}$ nanoparticle. While experimental verification of our predictions is currently not available, the results in Fig. 10 suggest that by appropriately tuning the nanoparticle composition and the support, it is possible to tailor the catalytic activity of supported metal nanoparticles. Toward improving selectivity, when single Pt atoms are required, the best choice would be $Pt_{125}Au_{125}$ nanoparticles on (10,10) CNTs. When chains of Pt atoms or isolated Pt atoms are required, $Pt_{125}Au_{125}$ nanoparticles on (13,13) CNTs are the best choice. When small islands of Pt are required, $Pt_{188}Au_{62}$ nanoparticles on (13,13) CNT bundles are the recommended catalyst, etc.

Experimental validation of our predictions could be attempted by extended x-ray-absorption fine structure (EXAFS), which yields the coordination number of surface atoms to be compared to our results, x-ray photoelectron spectroscopy (XPS), which yields the composition of a surface and may yield information about surface enrichment, and, more importantly, by spectroscopy analysis of CO adsorption. CO is expected to have different adsorption energies on metal atoms of different coordination, thus yielding different vibration frequencies. To enable the comparison between experimental and simulation data for vibration frequencies of adsorbed CO, we are conducting *ab initio* DFT calculations.

All of the changes in the arrangement of the surface atoms discussed above are related to the change in the curvature of the support. As can be seen in the snapshots in Fig. 8, nanoparticles on supports of different curvature have different shapes, a result which leads to different arrangements of atoms. To elucidate the molecular driving force for the observed results, we calculated the adsorption energy and the "deformation" energy for the nanoparticles on each of the supports. The adsorption energy is calculated by subtracting from the energy of the particle-plus-CNT-bundle system the sum of the energy of the nanoparticle in vacuum and that of the CNT bundle without the nanoparticle. The deformation energy is the difference between the energy of the supported nanoparticle, deformed by the CNT bundle, and the energy of the nanoparticle in vacuum. The results for the adsorption energy are reported in Fig. 11 and indicate that the adsorption energy depends strongly on both the nanoparticle composition and the support geometry. The most favorable adsorption occurs on the (20,20) CNTs, likely because the nanoparticles are "sandwiched" between neighboring CNTs and consequently more atoms interact with carbon atoms

(see snapshots in Fig. 1). The results for the "deformation" energy, reported in Fig. 12, show that any of the supports considered here deform the nanoparticles. The deformation energy for the nanoparticles is largest on the (20,20) CNT bundle, where the adsorption energy is the most negative (see Fig. 11). These results demonstrate that the support actively affects the properties of the supported nanoparticles and therefore affects the distribution of metal atoms on the nanoparticle surface.

IV. CONCLUSIONS

We have conducted all-atom molecular dynamics simulations of bimetallic Pt-Au nanoparticles supported by graphite and bundles of carbon nanotubes of various radii. The embedded-atom method, Lennard-Jones potential, and the Tersoff potential were used to model metal-metal, metal-carbon, and carbon-carbon interactions, respectively. We have found that $Pt_{125}Au_{125}$ nanoparticles form a well-defined Pt-Au core-shell structure and that the support slightly affects the atomic segregation within the nanoparticle. $Pt_{62}Au_{188}$ and $Pt_{188}Au_{62}$ nanoparticles form structures with a mixed Pt-Au core surrounded by an Au shell and a Pt core covered by a mixed Pt-Au shell, respectively. The support affects not only the number of Pt atoms on the nanoparticles surface, but also their arrangement. For $Pt_{188}Au_{62}$ nanoparticles, the number of Pt atoms on the nanoparticles surface decreases when the nanoparticles are supported on bundles of carbon nanotubes. For $Pt_{62}Au_{188}$ nanoparticles, the maximum number of Pt atoms is found when the nanoparticles are supported on bundles of (13,13) CNTs. For $Pt_{125}Pt_{125}$ nanoparticles, the minimum number of Pt atoms on the surface is found when the nanoparticles are either unsupported or supported by bundles of (20,20) CNTs. Our calculations suggest that because the supports deform the supported nanoparticles, they determine changes in surface properties. Because of their importance in catalytic applications, we also studied the size of the clusters of Pt atoms on the nanoparticles' surface. Our results show that changing the support geometry alters the distribution of the sizes of the surface clusters, especially for $Pt_{188}Au_{62}$ nanoparticles. Because the coordination states of the surface atoms are also affected by the support, our results suggest that it should be possible to tailor the distribution of atoms in bimetallic nanoparticles by careful selection of the nanoparticle composition and geometry of the support, with important implications in controlling the selectivity of catalysts.

ACKNOWLEDGMENTS

The authors acknowledge financial support from the Carbon Nanotube Technology Center (CANTEC) at the University of Oklahoma, funded by the U.S. DOE under Contract No. DE-FG02-06ER64239. Generous allocations of computing time were provided by the OU Supercomputing Center for Education and Research (OSCER) at the University of Oklahoma and by the National Energy Research Scientific Computing Center (NERSC) at Lawrence Berkeley National Laboratory. The authors acknowledge fruitful discussions with Friederike Jentoft, Richard Mallinson, and Daniel Resasco of the University of Oklahoma.

*Author to whom all correspondence should be addressed. FAX: 405 325 5813; astriolo@ou.edu

[1] R. Ferrando, J. Jellinek, and R. L. Johnston, Chem. Rev. **108**, 845 (2008).
[2] J. Luo, P. N. Njoki, Y. Lin, D. Mott, L. Wang, and Zhong, Langmuir **22**, 2892 (2006).
[3] J. Luo, M. M. Maye, N. N. Kariuki, L. Wang, P. Njoki, Y. Lin, M. Schadt, H. R. Naslund, and C.-J. Zhong, Catal. Today **99**, 291 (2005).
[4] P. B. Balbuena, Y. Wang, E. J. Lamas, S. R. Calvo, L. A. Agapito, and J. M. Seminario, in *Device and Materials Modeling in PEM Fuel Cells*, edited by S. J. Paddison and K. S. Promislow (Springer, Heidelberg, 2009), Vol. 113, pp. 509–532.
[5] C.-J. Zhong, J. Luo, P. N. Njoki, D. Mott, B. Wanjala, R. Loukrakpam, S. Lim, L. Wang, B. Fang, and Z. Xu, Energy Environ. Sci. **1**, 454 (2008).
[6] J. Luo, P. N. Njoki, Y. Lin, L. Wang, and C. J. Zhong, Electrochem. Commun. **8**, 581 (2006).
[7] Y. Shu, L. E. Murillo, J. P. Bosco, W. Huang, A. I. Frenkel, and J. G. Chen, Appl. Catal., A **339**, 169 (2008).
[8] A. B. Merlo, V. Vetere, J. F. Ruggera, and M. L. Casella, Catal. Commun. **10**, 1665 (2009).
[9] A. J. Plomp, D. M. P. van Asten, A. M. J. van der Eerden, P. Mäki-Arvela, D. Y. Murzin, K. P. de Jong, and J. H. Bitter, J. Catal. **263**, 146 (2009).
[10] N. M. Bertero, A. F. Trasarti, B. Moraweck, A. Borgna, and A. J. Marchi, Appl. Catal., A **358**, 32 (2009).
[11] J. M. Thomas, R. D. Adams, E. M. Boswell, B. Captain, H. Grönbeck, and R. Raja, Faraday Discuss. **138**, 301 (2008).
[12] M. O. Nutt, J. B. Hughes, and M. S. Wong, Environ. Sci. Technol. **39**, 1346 (2005).
[13] F. He, D. Zhao, J. Liu, and C. B. Roberts, Ind. Eng. Chem. Res. **46**, 29 (2007).
[14] J. L. Fernandez, D. A. Walsh, and A. J. Bard, J. Am. Chem. Soc. **127**, 357 (2005).
[15] Y. Zhao, Y. E. L. Fan, Y. Qiu, and S. Yang, Electrochim. Acta **52**, 5873 (2007).
[16] B. Yoon, H.-B. Pan, and C. M. Wai, J. Phys. Chem. C **113**, 1520 (2009).
[17] S. Linic, J. Jankowiak, and M. A. Barteau, J. Catal. **224**, 489 (2004).
[18] F. Studt, F. Abild-Pedersen, T. Bligaard, R. Z. Sorensen, C. H. Christensen, and J. K. Norskov, Science **320**, 1320 (2008).
[19] B. H. Morrow and A. Striolo, J. Phys. Chem. C **111**, 17905 (2007).
[20] B. H. Morrow and A. Striolo, Nanotechnology **19**, 195711 (2008).
[21] Y. Shao, G. Yin, Y. Gao, and P. Shi, J. Electrochem. Soc. **153**, A1093 (2006).
[22] S.-P. Huang, D. S. Mainardi, and P. B. Balbuena, Surf. Sci. **545**,

163 (2003).
[23] W. D. Luedtke and U. Landman, Phys. Rev. Lett. **82**, 3835 (1999).
[24] L. J. Lewis, P. Jensen, N. Combe, and J. L. Barrat, Phys. Rev. B **61**, 16084 (2000).
[25] P. Jensen, A. Clément, and L. J. Lewis, Physica E (Amsterdam) **21**, 71 (2004).
[26] S.-P. Huang and P. B. Balbuena, Mol. Phys. **100**, 2165 (2002).
[27] S. Y. Liem and K.-Y. Chan, Surf. Sci. **328**, 119 (1995).
[28] G.-W. Wu and K.-Y. Chan, Surf. Sci. **365**, 38 (1996).
[29] Z. Gu and P. B. Balbuena, Catal. Today **105**, 152 (2005).
[30] J. Chen and K.-Y. Chan, Mol. Simul. **31**, 527 (2005).
[31] E. J. Lamas and P. B. Balbuena, J. Phys. Chem. B **107**, 11682 (2003).
[32] S. K. R. S. Sankaranarayanan, V. R. Bhethanabotla, and B. Joseph, Phys. Rev. B **72**, 195405 (2005).
[33] B. Yoon, W. D. Luedtke, J. Gao, and U. Landman, J. Phys. Chem. B **107**, 5882 (2003).
[34] G.-W. Wu and K.-Y. Chan, Surf. Rev. Lett. **4**, 855 (1997).
[35] G.-W. Wu and K.-Y. Chan, J. Electroanal. Chem. **450**, 225 (1998).
[36] S. H. Lee, S. S. Han, J. K. Kang, J. H. Ryu, and H. M. Lee, Surf. Sci. **602**, 1433 (2008).
[37] J. H. Ryu, D. H. Seo, D. H. Kim, and H. M. Lee, Phys. Chem. Chem. Phys. **11**, 503 (2009).
[38] D. H. Seo, H. Y. Kim, J. H. Ryu, and H. M. Lee, J. Phys. Chem. C **113**, 10416 (2009).
[39] D. H. Kim, H. Y. Kim, J. H. Ryu, and H. M. Lee, Phys. Chem. Chem. Phys. **11**, 5079 (2009).
[40] S. J. Mejia-Rosales, C. Fernandez-Navarro, E. Perez-Tijerina, J. M. Montejano-Carrizales, and M. Jose-Yacaman, J. Phys. Chem. B **110**, 12884 (2006).
[41] H. B. Liu, U. Pal, R. Perez, and J. A. Ascencio, J. Phys. Chem. B **110**, 5191 (2006).
[42] G. Li, Q. Wang, D. Li, X. Lü, and J. He, Mater. Chem. Phys. **114**, 746 (2009).
[43] S. K. R. S. Sankaranarayanan, V. R. Bhethanabotla, and B. Joseph, Phys. Rev. B **71**, 195415 (2005).
[44] H. B. Liu, U. Pal, and J. A. Ascencio, J. Phys. Chem. C **112**, 19173 (2008).
[45] Z. Yang, X. Yang, and Z. Xu, J. Phys. Chem. C **112**, 4937 (2008).
[46] O. A. Oviedo, E. P. M. Leiva, and M. M. Mariscal, Phys. Chem. Chem. Phys. **10**, 3561 (2008).
[47] S. Xiao, W. Hu, W. Luo, Y. Wu, X. Li, and H. Deng, Eur. Phys. J. B **54**, 479 (2006).
[48] S. J. Mejia-Rosales, C. Fernandez-Navarro, E. Perez-Tijerina, D. A. Blom, L. F. Allard, and M. Jose-Yacaman, J. Phys. Chem. C **111**, 1256 (2007).
[49] F. Chen and R. L. Johnston, Appl. Phys. Lett. **92**, 023112 (2008).
[50] Y. H. Chui and K.-Y. Chan, Mol. Simul. **30**, 679 (2004).
[51] Y. H. Chui and K.-Y. Chan, Chem. Phys. Lett. **408**, 49 (2005).
[52] D. H. Kim, H. Y. Kim, H. G. Kim, J. H. Ryu, and H. M. Lee, J. Phys.: Condens. Matter **20**, 035208 (2008).
[53] M. M. Mariscal, S. A. Dassie, and E. P. M. Leiva, J. Chem. Phys. **123**, 184505 (2005).
[54] H. B. Liu, U. Pal, A. Medina, C. Maldonado, and J. A. Ascencio, Phys. Rev. B **71**, 075403 (2005).
[55] S. R. Calvo and P. B. Balbuena, Surf. Sci. **581**, 213 (2005).
[56] N. Dimitratos, C. Messi, F. Porta, L. Prati, and A. Villa, J. Mol. Catal. A: Chem. **256**, 21 (2006).
[57] M. Comotti, C. D. Pina, and M. Rossi, J. Mol. Catal. A: Chem. **251**, 89 (2006).
[58] X. Guo, D.-J. Guo, X.-P. Qiu, L.-Q. Chen, and W.-T. Zhu, Electrochem. Commun. **10**, 1748 (2008).
[59] *CRC Handbook of Chemistry and Physics*, 84th ed., edited by D. R. Lide (CRC Press, Boca Raton, 2003).
[60] S. Plimpton, J. Comput. Phys. **117**, 1 (1995).
[61] M. P. Allen and D. J. Tildesley, *Computer Simulation of Liquids* (Oxford University Press, Oxford, 2004).
[62] S. M. Foiles, M. I. Baskes, and M. S. Daw, Phys. Rev. B **33**, 7983 (1986).
[63] M. S. Daw, S. M. Foiles, and M. I. Baskes, Mater. Sci. Rep. **9**, 251 (1993).
[64] O. S. Trushin, P. Salo, and T. Ala-Nissila, Phys. Rev. B **62**, 1611 (2000).
[65] A. Sebetci and Z. B. Güvenç, Surf. Sci. **525**, 66 (2003).
[66] J. Tersoff, Phys. Rev. B **37**, 6991 (1988).
[67] J. Tersoff and R. S. Ruoff, Phys. Rev. Lett. **73**, 676 (1994).
[68] J. Zang, O. Aldas-Palacios, and F. Liu, Comm. Comp. Phys. **2**, 451 (2007).
[69] A. N. Imtani and V. K. Jindal, Phys. Rev. B **76**, 195447 (2007).
[70] J.-Y. Hsieh, J.-M. Lu, M.-Y. Huang, and C.-C. Hwang, Nanotechnology **17**, 3920 (2006).
[71] N. R. Raravikar, P. Keblinski, A. M. Rao, M. S. Dresselhaus, L. S. Schadler, and P. M. Ajayan, Phys. Rev. B **66**, 235424 (2002).
[72] V. R. Bhethanabotla and W. A. Steele, Phys. Rev. B **41**, 9480 (1990).
[73] P. M. Agrawal, B. M. Rice, and D. L. Thompson, Surf. Sci. **515**, 21 (2002).
[74] C. K. Acharya, D. I. Sullivan, and C. H. Turner, J. Phys. Chem. C **112**(35), 13607 (2008).
[75] B. H. Morrow and A. Striolo, Mol. Simul. **35**, 795 (2009).
[76] Z. Yang, X. Yang, Z. Xu, and S. Liu, Phys. Chem. Chem. Phys. **11**, 6249 (2009).
[77] J. A. Reyes-Nava, J. L. Rodriguez-Lopez, and U. Pal, Phys. Rev. B **80**, 161412 (2009).
[78] A. Henglein, J. Phys. Chem. B **104**, 2201 (2000).
[79] J. H. Hodak, A. Henglein, and G. V. Hartland, J. Chem. Phys. **114**, 2760 (2001).
[80] D. I. Garcia-Gutierrez, C. E. Gutierrez-Wing, L. Giovanetti, J. M. Ramallo-Lopez, F. G. Requejo, and M. Jose-Yacaman, J. Phys. Chem. B **109**, 3813 (2005).
[81] J. Yang, J. Yang Lee, and H.-P. Too, Plasmonics **1**, 67 (2006).
[82] S. Wang, N. Kristian, S. Jiang, and X. Wang, Nanotechnology **20**, 025605 (2009).
[83] W. Zhang, L. Li, Y. Du, X. Wang, and P. Yang, Catal. Lett. **127**, 429 (2009).